JOURNAL OF PROPULSION AND POWER
Vol. 31, No. 1, January–February 2015

Effect of Addition of Energetic Nanoparticles on Droplet-Burning Rate of Liquid Fuels

Saad Tanvir* and Li Qiao*
Purdue University, West Lafayette, Indiana 47907

DOI: 10.2514/1.B35500

A droplet stream combustion experiment was developed to understand the effect of reducing droplet size to a micrometer scale on the combustion characteristics of nanofluid fuels, which are liquid fuels with a stable suspension of nanoparticles. Pure ethanol and ethanol with aluminum nanoparticles at varying concentrations (up to 5 wt%) and droplet sizes were studied. The effect of particle addition on the droplet-burning rate was determined, and the mechanisms that are responsible for that effect were identified. The results show that the droplet-burning rate increases with increasing particle concentration. For example, with a 5 wt% addition of 80 nm aluminum nanoparticles, the burning rate increased by 140%. The burning rate enhancement is mainly attributed to strong radiation absorption of the nanoparticles suspended within the droplets, which provides more energy from the exothermic reaction (the flame) to the liquid phase (the droplets) for vaporization, thus increasing the burning rate. The radiation absorption effect becomes increasingly important as the droplet size increases.

Nomenclature

B	=	Spalding transfer number
C_p	=	specific heat, J/kg · K
D	=	droplet diameter, m
D_0	=	initial droplet diameter, m
K	=	droplet-burning rate, mm^2/s
K_p	=	Planck mean absorption coefficient
k_p	=	Planck absorption coefficient
L_e	=	penetrating length for radiation, m
m	=	molar constant
Q	=	heat of combustion, W
Q_c	=	rate of heat transfer via conduction, W
Q_{f-s}	=	rate of heat entering the nanofluid droplet, W
Q_{rad}	=	rate of heat transfer via radiation, W
R_d	=	radius of the droplet, m
T	=	temperature, K
t	=	time, s
$Y_{O\infty}$	=	ratio of the mass fraction of air
η	=	burning rate correction factor
λ	=	thermal conductivity, W/m · K
ρ	=	density, kg/m^3
σ	=	Stefan–Boltzmann constant (5.67×10^{-8} $W/m^2 K^4$)

I. Introduction

HIGH-PERFORMANCE nanofluid-type fuels (liquid fuels with stable suspension of nanometer-sized particles) have received increasing interest recently. Energetic nanoparticles such as aluminum (Al) have high combustion energy and have been used as additives in propellants and explosives. Compared to micrometer-sized particles, nanoparticles offer a shortened ignition delay, a faster burning rate, and more complete combustion [1,2]. The unique properties of nanoparticles could be used to enhance the performance of current energy conversion systems when properly mixed with traditional liquid fuels, e.g., improving the power output of propulsion systems and enhancing ignition [3,4].

Presented as Paper 2013-3771 at the 49th AIAA/ASME/SAE/ASEE Joint Propulsion Conference, San Jose, CA, 14 July 2013–17 July 2014; received 25 June 2014; revision received 28 August 2014; accepted for publication 29 August 2014; published online 1 December 2014.

*School of Aeronautics and Astronautics.

Studies on the ignition and burning behaviors of nanofluid-type fuels, however, are scarce. Tyagi et al. [5] studied the ignition properties of Al/diesel and Al_2O_3/diesel fuels using a simple hot-plate experiment. The results showed enhancement in ignition probability as compared to pure diesel fuels alone. Beloni et al. [6] studied the effect of adding metallic additives such as Al, alloyed $Al_{0.7}Li_{0.3}$, and nanocomposites 2B + Ti to decane on flame length, flame speed, emissions, and temperature over a lifted laminar flame burner. Allen et al. [7] found that the addition of a small amount of Al nanoparticles to n-dodecane and ethanol in a shock tube significantly reduces the ignition delay time of both fuels. Van Devener et al. [3] and Van Devener and Anderson [4] studied the ignition and combustion of JP-10 (Exo-Tetrahydro Dicyclopentadiene) with the addition of CeO_2 nanoparticles and, later, boron nanoparticles coated with a CeO_2 catalytic layer. The results showed a significant reduction in the ignition temperature of JP-10. Rotavera et al. [8] found that the addition of CeO_2 nanoparticles in toluene significantly reduced soot deposition on the shock tube walls under high-fuel-concentration conditions.

Sabourin et al. [9,10] investigated the burning characteristics of monopropellants consisting of liquid nitromethane and nanoparticles of silicon- and aluminum-based oxides. The results showed that a small addition of silica or alumina results in a substantial increase in burning rate. This is attributed to the nanoparticles having a significantly large surface area that increases the rate of nitromethane decomposition. McCown and Petersen [11] later explored the effect of adding higher-energy density metallic nanoparticles such as Al on the burning rate of nitromethane and found a 5 wt% addition of Al resulted in a burning rate increase by 71–300%, depending on the operating pressure. It was hypothesized that enhanced heat transport through radiation absorption and emission by the nanoparticles was one of the mechanisms responsible for this behavior.

Gan et al. [12] explored the burning characteristics of single fuel droplets (in the range of 0.5–2.5 mm in diameter) containing nano- and microsized Al particles. For the same particle concentrations, the microexplosive behavior was more aggressive in the micro-suspensions as compared to the nanosuspensions. This was attributed to the difference in the structure of the agglomerates formed during the evaporation and combustion process. Gan and Qiao [13] later studied the combustion behavior of boron- and iron-based nanofluid fuels because boron and iron have higher-energy densities than Al. The burning behaviors of dilute and dense suspensions were compared. For dense nanosuspensions, most particles were burned as a large agglomerate at a later stage when all the liquid fuel had been consumed. Sometimes, this agglomerate may not burn if the energy provided by the droplet flame is insufficient. For dilute suspensions, the burning characteristics were characterized by a simultaneous

burning of both the droplet and the particles, which integrated into one stage.

These studies show that the combustion behavior of nanofluid-type fuels depends on multiple factors such as the type, size, and concentration of the nanoparticles added. Furthermore, the unique physical properties of nanofluids such as enhanced thermal conductivity and optical properties may also affect their burning behavior [14,15]. Earlier studies [12,13] examined the burning characteristics of large droplets in the range of 0.5–2.5 mm and found that particle aggregation plays an important role in the combustion behavior. However, for smaller droplets, such as in a spray, particle aggregation may be a less serious issue. This is because the aggregation timescale may be much longer than the characteristic droplet-burning timescale, which means that, until the droplet is completely evaporated and burned, the particles inside may have insufficient time to form a solid aggregate. This would essentially change the distinctive combustion stages and the overall burning characteristics. Another open question is how the addition of nanoparticles would affect the droplet-burning rate and what mechanisms are responsible for that effect.

Motivated by these, we developed a droplet stream combustion experiment that can produce a stream of droplets of micrometer size (100–500 μm) to understand the effect of droplet size on the combustion behavior of nanofluid fuels. The droplet-burning rate was measured for various particle concentrations and droplet sizes. The results show that a small amount of added nanoparticles can significantly increase the droplet-burning rate. A theoretical analysis was performed to observe that the absorption of the radiation energy emitted from the flame by the nanoparticles is mainly responsible for burning rate enhancement. The radiation absorption effect becomes increasingly important for larger droplets.

II. Experimental Methods

A. Fuel Preparation and Characterization

The nanofluid fuels are prepared using physical and chemical (where required) dispersion methodologies, as discussed in the earlier studies [12,13]. The appropriate amounts of particles were first vigorously stirred with the base fuel. This was followed by sonication of the colloidal mixture in an ultrasonic disrupter (Sharpertek, SYJ-450D) to minimize and delay particle agglomeration. The sonication was performed in an ice bath to maintain a constant temperature of the nanofluid. The sonicator generated a series of 4-s-long pulses with 4 s spacing. The mixture was sonicated for about 8 min.

Ethanol was used as a base fuel for the current study. Aluminum nanoparticles (with an average size of 80 nm, from Nanostructured and Amorphous Materials, Inc.) were considered as additives to the ethanol. Figure 1 shows the scanning electron microscopy (SEM) image of the nanoparticles. The amount of particles added was precisely measured using an analytical scale (Torban AGZN 100) with an accuracy of 0.1 mg. The nanofluid samples prepared (0.1–5 wt% aluminum in ethanol) maintained excellent suspension quality for over 2 h without the presence of a surfactant. This is because ethanol is a polar and hydrophilic liquid. Hence, a good suspension of nanoparticles with a hydrophilic oxide surface in ethanol is maintained.

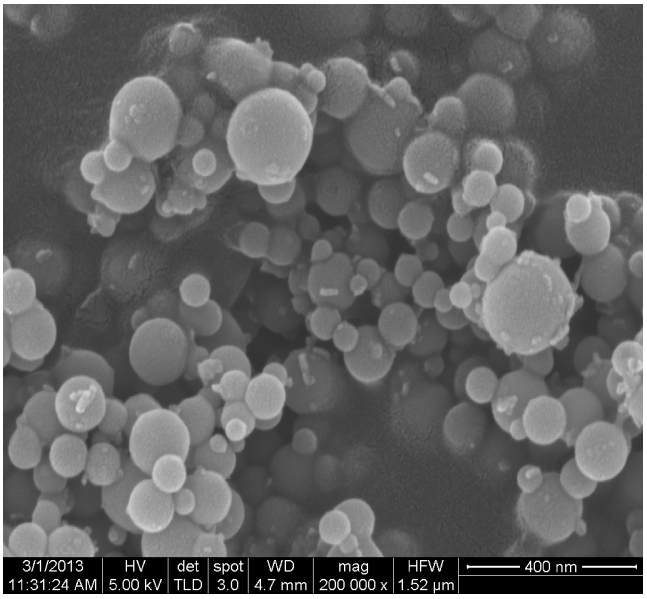

Fig. 1 SEM image of 80 nm aluminum particles.

B. Experimental Setup: The Droplet Stream Flame

The setup consists of a vibrating orifice droplet generator, a mechanical syringe pump system, a wave function generator, a linear amplifier, and a high-speed camera along with a backlight. The droplet generator (Drop Generator LHG-01), containing a piezoceramic disk and a customized orifice (the orifice diameter determines the size of the droplets), is oriented so that the stream is in a downward direction. A KD Scientific syringe pump system supplies the nanofluid fuel into the droplet generator at the specified constant volumetric flow rate via Festo PL-6 tubing. The wave function generator (model 519 AM/FM, function generator) is connected to the linear amplifier (Piezo Systems, Inc., model EPA-104) from which the signal is sent to both the piezoceramic disk inside the droplet generator as well as to the digital oscilloscope (Tektronix, TDS 2024B) to monitor the actual output of the amplifier.

As the fluid is forced through the droplet generator, the square wave signal causes the piezoceramic disk within the droplet generator to oscillate and apply longitudinal disturbances to the fluid jet, thus perturbing the fluid. In accordance with the Rayleigh instability theory, the fluid, when disturbed at the proper frequency, will break up from a uniform jet stream into a uniform stream of equally sized and spaced spherical droplets. A quantitative analysis was conducted on the stream to monitor droplet size and spacing as a function of applied frequency and volumetric flow rate using a high-speed digital camera.

A heated nickel coil, attached to a high-voltage power supply, was used to ignite the droplet streams. The coil was placed at a distance of 2 cm downstream of the orifice. A digital single-lens reflex camera was used to capture the burning behavior of the stream. A protective screen was placed around the flame to get better imaging and to isolate the flame from external air disturbances.

III. Results and Discussion

A. Thermophysical Properties of the Nanofluid Fuels

It is well known that nanofluids exhibit unique thermophysical properties that differ from those of the base fluid. For example, the addition of a small amount of nanoparticles into the base fluid can significantly increase the thermal conductivity of the fluid [16]. The thermal and physical properties of a fuel generally influence its combustion performance, and thus need to be characterized. Motivated by this, we experimentally determined properties including surface tension, viscosity, and thermal conductivity of the nanofluid fuels studied here. The results are discussed in the following.

A Rame-Hart model 500 standard goniometer, using the pendant drop method, was adapted to determine the surface tension of selected nanofluid fuels, as discussed in our previous work [17]. The method uses the Young–Laplace equation to determine the surface tension of the droplet based on the shape of the droplet. The results show that, for relatively low concentrations of Al nanoparticle addition (0–5 wt%), the surface tension of the nanofluid fuels shows a slight but negligible increase (less than 3%) versus the base fluid.

Thermal conductivity was measured using a KD2-Pro, from Decagon Devices, based on the transient line heat source method. The uncertainty was within $\pm 10\%$. The results (Table 1) show that, at room temperature, thermal conductivity increases as a function of increasing Al concentration. For example, with a 5 wt% addition of Al nanoparticles, thermal conductivity increases by 24%. The enhancement is not only due to the fact that metals have much higher thermal conductivity than fluids but could also be due to other

Table 1 Thermal conductivity variation as a function of Al particle concentration

Aluminum in ethanol, wt %	Thermal conductivity, W/m · K	Enhancement, %
0	0.176	0.00
1	0.198	12.53
3	0.215	22.44
5	0.218	24.03

mechanisms, as suggested by the literature, e.g., the formation of a layered structure which acts as a thermal bridge between a solid nanoparticle and a bulk liquid and particle aggregation [16].

The rheological properties of the nanofluid fuels were measured using a Stresstech rotational rheometer. A known shear strain was applied to the liquid, a corresponding shear stress was calculated, and vice versa. Once both the shear rate and shear stress were found, the rheometer calculated the viscosity. The experiments were conducted at room temperature. It was assumed that the temperature of the environment did not fluctuate during the experiments. Figure 2 shows the variation of the relative viscosity of the nanofluid fuels as a function of shear rate and particle concentration. It is seen that, up to a 5 wt% addition of Al nanoparticles, the viscosity remains relatively unchanged from that of pure ethanol. Upon further addition of nanoparticles, we begin to see an increase of 5 and 15% for 10 and 15 wt% nanofluids. Furthermore, at these higher concentrations, shear thinning behavior becomes more prominent. For this current work, we can assume that viscosity does not change significantly for dilute nanofluid fuels.

B. Flame Characteristics and Combustion Products Analysis

Droplet stream combustion experiments were conducted for pure ethanol and ethanol with the addition of up to 5 wt% Al nanoparticles. Two droplet sizes were considered: 176 and 400 μm. Figure 3 shows the image of a droplet stream flame for ethanol with 3 wt% Al. The burning process can be divided into two distinctive stages. Stage 1 is characterized by pure ethanol combustion, shown by the region of ethanol flame. In this stage, the droplets within the stream were uniformly distributed and undisturbed. As they fall, their size continues to decrease as a result of steady evaporation. Stage 2 is characterized by simultaneous combustion of both ethanol and Al nanoparticles, shown by flares that appear in the flame zone surrounded by the ethanol flame. The Al particles (and particle aggregates) are ejected from the droplets and brought to the droplet stream flame zone to burn, resulting in many local particle flames. The integrated burning behavior is similar to what was observed in previous work [12,13]. Furthermore, in this stage, the droplets inside the stream are no longer of uniform size and shape, nor are they at a constant distance from each other, as evidenced by Figs. 3c–3e. The microexplosive nature of the Al particles and aggregates causes disruption within the flame surrounding the droplets. As the disruption and microexplosion intensity increases, it compromises the uniformity of the stream.

Scanning electron microscopy and energy dispersive x-ray spectroscopy (EDX) analyses were performed on the combusted particles and their aggregates that were collected downstream of the flame. Figure 4 shows SEM images of deposits of burned Al for 1.0, 2.0, and 3.0 wt% Al in ethanol, respectively. As the Al nanoparticle concentration increases, the density and size of the combustion residues increase. For all cases, however, the sizes of the residues (less than 5 μm) are much smaller than the initial size of the droplet (176 μm). This indicates that, during the droplet-burning process, particles within the droplet did not have a chance to form a large aggregate and that aggregation may not play as significant a role as it does for millimeter-sized droplets.

In contrast, previous studies [12,13], which examined the effect of nanoparticle addition on the burning behavior of millimeter-sized droplets, found that nanoparticles had a tendency to form a large aggregate and that the large aggregate burned at a later stage after the liquid fuel had been completely combusted. Additionally, the size of the aggregate was of the same order of magnitude as the size of the droplet (millimeter). We have known that the particle aggregation process plays an important role in overall burning characteristics. For a large droplet, the characteristic time for particle aggregation may be on the same order as the characteristic time of droplet burning. However, for much smaller droplets, the aggregation timescale may be much longer than the characteristic droplet-burning timescale. This indicates that, until the droplet was completely evaporated and burned, the particles inside may not have had sufficient time to form a solid aggregate. This explains why the burning characteristics of large millimeter-sized droplets are different from smaller ones in the range of a few to a few hundred micrometers.

Furthermore, EDX analysis shows a consistent Al/O ratio for all three samples. The Al/O ratio is 0.65, 0.66, and 0.6 for 1, 2, and 3 wt% Al, respectively, indicating complete combustion of Al. This is possible due to the small size of the Al particles and aggregates allowing more surface area to be exposed to the flame to burn completely. Lastly, we found that the distance at which the particles began to escape from the droplet stream and to burn varies with particle concentration. It increases with increasing particle concentration, as shown in Fig. 5. This is likely due to the faster evaporation rate (or surface regression rate) of the droplets at higher particle concentrations, which causes the particles to escape from the

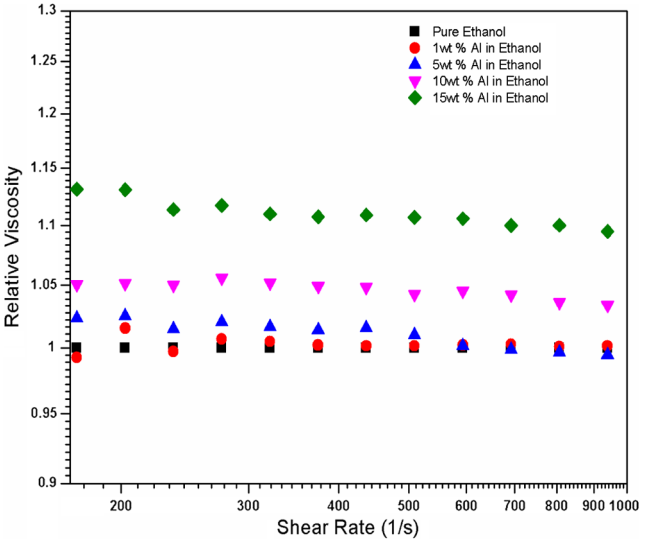

Fig. 2 Variation of relative viscosity as a function of shear rate and Al nanoparticle concentration.

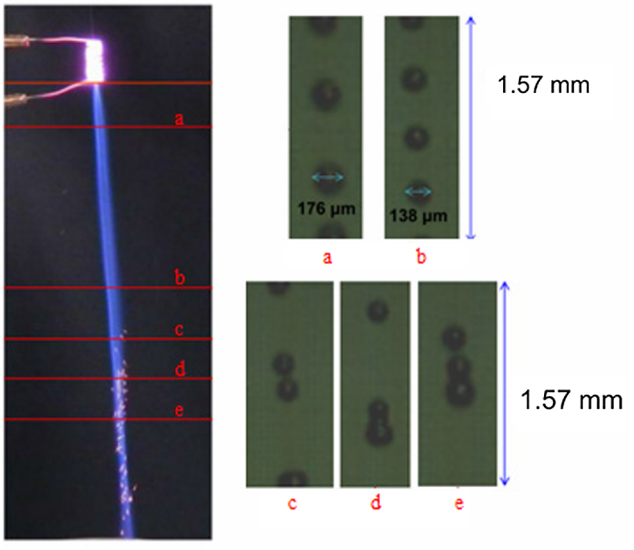

Fig. 3 (left) 3 wt% Al/ethanol flame; (right) (a, b) pure ethanol combustion and (c–e) simultaneous combustion.

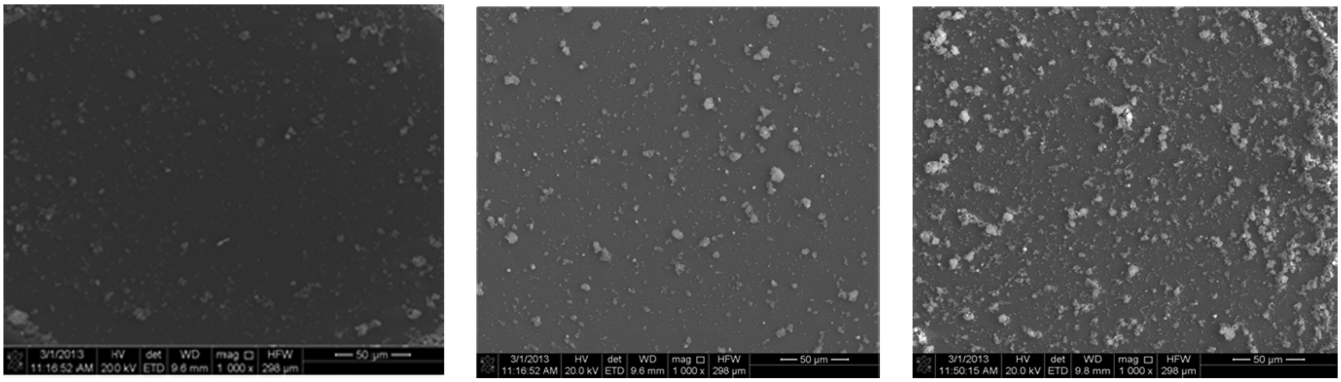

a) b) c)

Fig. 4 SEM images of combustion residues of burned Al particles and aggregates: a) 1 wt% Al in ethanol; b) 2 wt% Al in ethanol; and c) 3 wt% Al in ethanol.

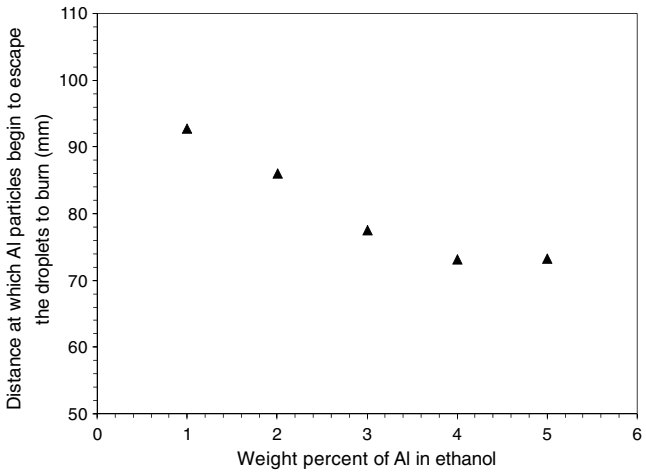

Fig. 5 Distance at which Al particles begin to escape the droplet stream flame as a function of Al concentration in ethanol for the droplets with an initial size of 400 μm.

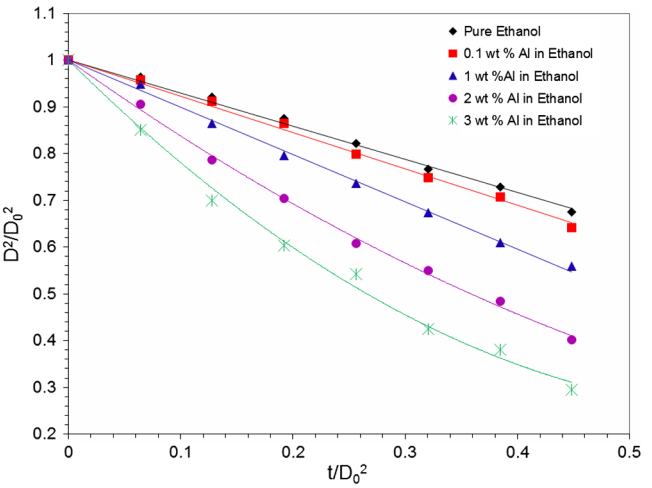

Fig. 6 Variation of droplet diameter squared as a function of time for the ethanol-based nanofluid fuels with varying Al concentrations for an initial droplet size of 176 μm.

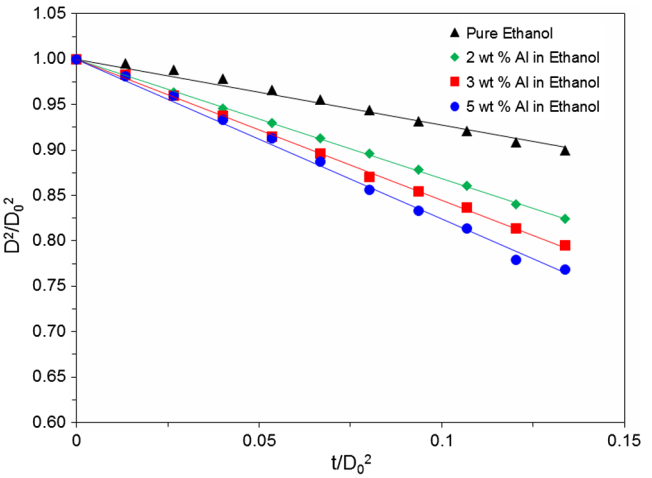

Fig. 7 Variation of droplet diameter squared as a function of time for the ethanol-based nanofluid fuels with varying Al concentrations for an initial droplet size of 400 μm.

droplet stream flame earlier. Nevertheless, further insight into the escape mechanisms of particles from droplets will help explain this phenomenon better.

C. Effect of Particle Addition on Droplet-Burning Rate

The droplet-burning rate was determined by measuring droplet sizes at periodic locations downstream of the ignition coil using backlight shadowgraphy technique. As described earlier, at a certain distance downstream of the ignition coil, particles and particle aggregates started to escape from the droplets and to burn. As a result, the stream was disrupted and could no longer remain stable and uniform. Thus, the measurements of the droplet sizes were taken only in regions where the droplet stream was uniform and stable.

Figures 6 and 7 show the variation of droplet diameter squared as a function of time for ethanol, with varying Al concentrations for 176 μm droplets (at a spacing of 550 μm) and 400 μm droplets (at a spacing of 1035 μm), respectively. Starting with 12.5 mm downstream from the end of the ignition coil, the measurements were taken in increments of 12.5 mm downstream of the flame. The speeds of the falling droplets within the stream were determined using the high-speed camera and were estimated to be 6.37 and 11.8 m/s, respectively.

For the 176 μm droplets (Fig. 6), the square of the droplet size decreased linearly with time for pure ethanol and for ethanol with low concentrations of Al particles (0.1–2.0 wt%), following the classical D^2-law. This is consistent with the works of Botero et al. [18,19], which showed that freely falling droplets of fuel blends and mixtures observed the D^2 law of droplet regression. This is because, once the temperature at the droplet surface reaches the boiling point of the surface species, the fuel volatility no longer impacts the fuel vapor concentration, and thereby the fuel gasification rate. As the particle concentration increases, however, the droplet size regression deviates slightly from the D^2 law. This behavior could be attributed to multiple factors, e.g., the aggregation of nanoparticles, as suggested by Gan

Qiao [14]. As the particle concentration increases, the degree of aggregation also increases. The large aggregation structures impede the fluid flow from the droplet interior to the surface, and thus reduce the vaporization rate. Other factors, such as the variation of physical properties (such as viscosity and surface tension) resulting from the addition of particles, may also alter the apparent heat of vaporization, and consequently change the vaporization rate.

For the 400 μm droplets, the square of the droplet size decreases linearly with time for all cases. Even for high particle concentrations, such as 3 and 5 wt%,. the droplets regress while obeying the D^2 law of combustion approximately. Previous studies of the droplet combustion on slurry fuels also showed that the droplet surface regression rate follows the D^2 law for droplets of sizes ranging from 0.8 to 2 mm in diameter [13,20]. However, earlier, we noticed that, as the particle concentration reached 3 wt% for the 176 μm droplets, the burning behavior started to deviate slightly from the D^2 law. These observations indicate that, as the droplet size decreases, the influence of particle addition on droplet evaporation and the burning rate becomes increasingly important, especially at high loading rates.

Figure 8 shows the burning rate as a function of Al particle concentration for the 176 and 400 μm droplets, respectively. The average burning rates of pure ethanol are 0.72 and 0.74 mm^2/s for the two initial droplets sizes, respectively. The slight increase can be attributed to the increased spacing between the droplets. When the droplet size increases from 176 to 400 μm, the spacing parameter C (ratio of interdroplet distance to droplet diameter) changes from 2.5 to 3.2. With increasing C, the burning rate become closer to that of an isolated droplet of the same diameter, which is higher than that of a droplet in a stream [21]. Clearly, the addition of Al nanoparticles increases droplet-burning rate. For example, with a 5 wt% addition of Al particles, the burning rate increased by 140%. Such enhancement is significant, considering only a small amount of Al particles were added to the base fuel. The possible mechanisms responsible for the enhancement will be discussed in the next section. It can also be seen from Fig. 8 that, for the 5 wt% Al case, the burning rate deviates from the otherwise linear relationship between the particle concentration and the burning rate. It is believed that the particle aggregation present within the droplets at a higher concentration plays a part in reducing the rate of increase of the regression rate. As mentioned earlier, aggregates tend to impede fluid flow to the surface, resulting in a reduction in regression rate. Lastly, we found that the burning rate is nearly independent of droplet size, which is consistent with Okajima and Kumagai's [22] work, which showed ethanol burning rates did not vary significantly as a function of initial droplet diameter.

D. Mechanisms for Droplet-Burning Rate Enhancement

Several mechanisms could potentially explain the burning rate enhancement phenomenon as a result of particle addition, e.g., reduction in surface tension and surface energy at the liquid/gas interface, radiation absorption of nanoparticles, and a physical interaction between the high-surface-area particles and ethanol (wetting) increasing the interface area between the gas and liquid phases. It is not clear which mechanism is dominant under various conditions.

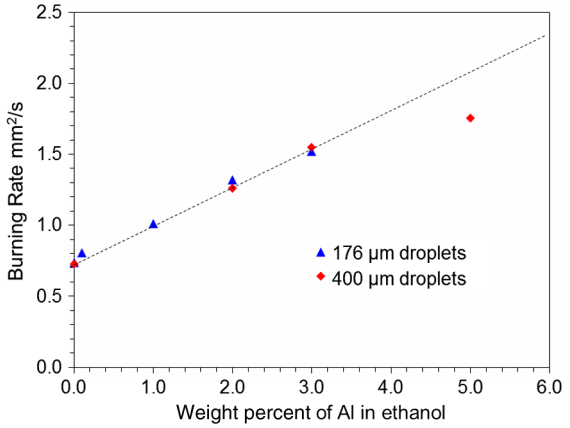

Fig. 8 Variation of droplet-burning rate as a function of Al nanoparticle concentration for the 176 and 400 μm dropletsm respectively.

To understand the effects of a nanoparticles addition on the droplet-burning rate, we considered the classical combustion model of a single droplet, in which the burning rate constant K can be expressed as [23]

$$K = \frac{4\pi k_g r_s}{C_{pg}} \ln(1 + B) \tag{1}$$

where k_g is the thermal conductivity of the gases surrounding the droplet, C_{pg} is the specific heat of the gases, and B is the Spalding transfer number. Both k_g and C_{pg} can be assumed to be independent of the nanoparticle concentration because they are gas phase quantities. B can be expressed as a function of C_{pg}, the heat of combustion Q, the ratio of the mass fraction of air $Y_{O\infty}$, the molar constant m, and the overall latent heat of vaporization H:

$$B = \frac{C_{pg}(T_\infty - T_s) + (Y_{0\infty}/m)Q}{H} \tag{2}$$

B can be further simplified by assuming that $H \ll Q$, and the ratio of the mass fraction of air $Y_{O\infty}$ to the molar constant m is much lower than one; we can then state the following [23]:

$$B \approx \frac{C_{pg}(T_f - T_s)}{H} \tag{3}$$

First of all, because of the additional heat release from the Al particle burning, which took place 70–85 mm downstream of the ignition coil, the flame temperature of ethanol with Al particles should be higher than that of pure ethanol. This may cause the droplet-burning rate to increase because of higher T_f. To quantify this effect, we calculated the increase in the flame temperature of an ethanol/Al fuel mixture using the NASA CEA online software.[†] Here, we assumed bulk Al and that all of the Al burns simultaneously with ethanol. The results show that, with all other properties kept constant, the flame temperature increases from 2194 K for pure ethanol to 2280 K for ethanol with 5 wt% Al. As a result of the higher flame temperature, the droplet-burning rate increases by 6% according to Eq. (3). The 6% increase, however, is much smaller than the actual increase of 140%, as shown in Fig. 8. Thus, we can conclude that the flame temperature increase because of Al particle burning is not the dominant mechanism for the droplet-burning rate enhancement.

Note that the classical droplet combustion model [Eqs. (1–3)] takes into account the heat transfer from the flame to the droplet surface via thermal conduction only. Radiative heat transfer (radiation absorbed by the droplet) is usually neglected because most liquid fuels are transparent to the radiation emitted from a flame. It, however, may become significant for nanofluid fuels because the nanoparticles suspended in the droplet can absorb the radiation energy emitted from the flame. Fundamentally, more heat transfer from the exothermic chemical reactions (flame) back to the liquid phase (droplet) would increase the droplet-burning rate, as it provides more energy per unit time needed to vaporize the liquid fuel. To test the hypothesis that radiation absorption by the nanoparticles is a main mechanism for droplet-burning rate enhancement, we developed a simple model, as described next.

Figure 9 shows a sketch of the energy balance for a burning nanofluid droplet. The total heat transfer to the droplet from the flame consists of two parts: conductive heat Q_{cond}, and radiation absorption by the nanoparticles Q_{rad}. Here, we neglected the radiation absorption by the liquid part of the droplet. The conductive heat transfer can be expressed as

[†]Data available online at http://www.grc.nasa.gov/WWW/CEAWeb/ceaHome.htm [retrieved 2014].

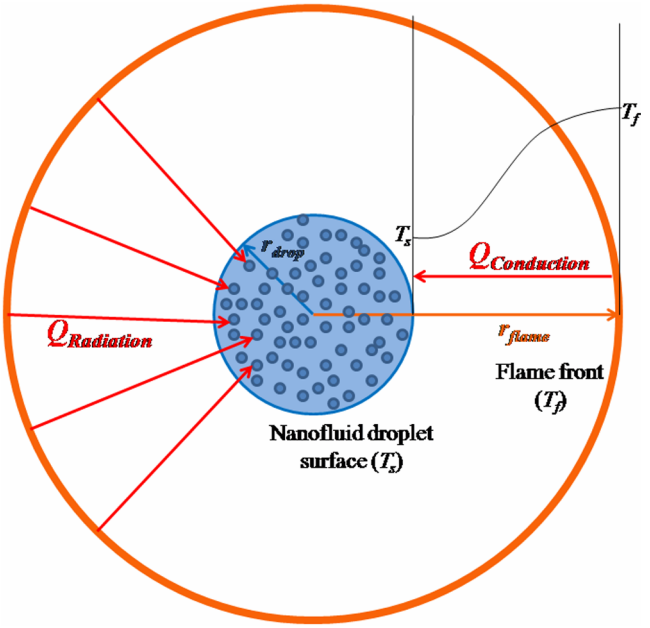

Fig. 9 Energy balance around a burning nanofluid droplet.

$$Q_{\text{cond}} = \left(4\pi r^2 \lambda_g \frac{\partial T}{\partial r}\right)_s = \dot{m}_f \times H \tag{4}$$

where r is the droplet radius, and λ_g is the thermal conductivity of the gases in the region between the flame and the droplet surface. From tabulated, mass-weighted, and temperature-averaged thermal conductivities of the gaseous mixture surrounding the droplet and inward of the flame, λ_g was determined. The magnitude of the conductive heat transfer was comparable to the energy used for vaporization of pure ethanol ($\dot{m}_f \times H$), where $\dot{m}_f$ is the mass flow rate of vaporization and H is the latent heat of the evaporation of ethanol. The mass flow rate of vaporization $\dot{m}_f$ was determined using the experimental results shown in Figs. 6 and 7.

To estimate the amount of radiation emitted from the flame that was absorbed by the particles suspended in the droplet, an optically thin model [24] was used. It can be expressed as

$$Q_{\text{rad}} = 4\sigma K_p A L_E (T_f^4 - T_s^4) \tag{5}$$

where σ is the Stefan–Boltzmann constant, L_E is the penetrating length (which can be assumed to be the radius of the stream flame; about 3 mm), A is the surface area of all the particles in the droplet, and K_p denotes the Planck mean absorption coefficient. K_p was found using the partial pressures and the Planck absorption coefficients of each contributing gaseous species, as shown in Eq. (6):

$$K_p = \sum_{i=1}^{N} P_i k_{p_i} \tag{6}$$

where P_i represents the partial pressure of species i. Assuming a flame temperature of 2200 K (based on the NASA CEA calculations of stoichiometric combustion of ethanol in air), the values of k_p can be obtained from tabulated results found in [25]. CO_2 and H_2O are the only species considered in the combustion products, and they contribute most to the radiation emission from the flame.

For this simple model, we also assume that the temperature at the droplet surface is equal to the boiling point of ethanol ($T_s = T_b = 351$ K). We also assume that Al particles behave as a blackbody receiver, meaning that all the radiation emitted from the flame is absorbed by the Al nanoparticles. This is a reasonable assumption because Gan and Qiao [15] measured the transmission spectrum of ethanol with Al nanoparticles in the range of 200–900 nm and found that 0.1 wt% Al in ethanol transmitted only 2% of

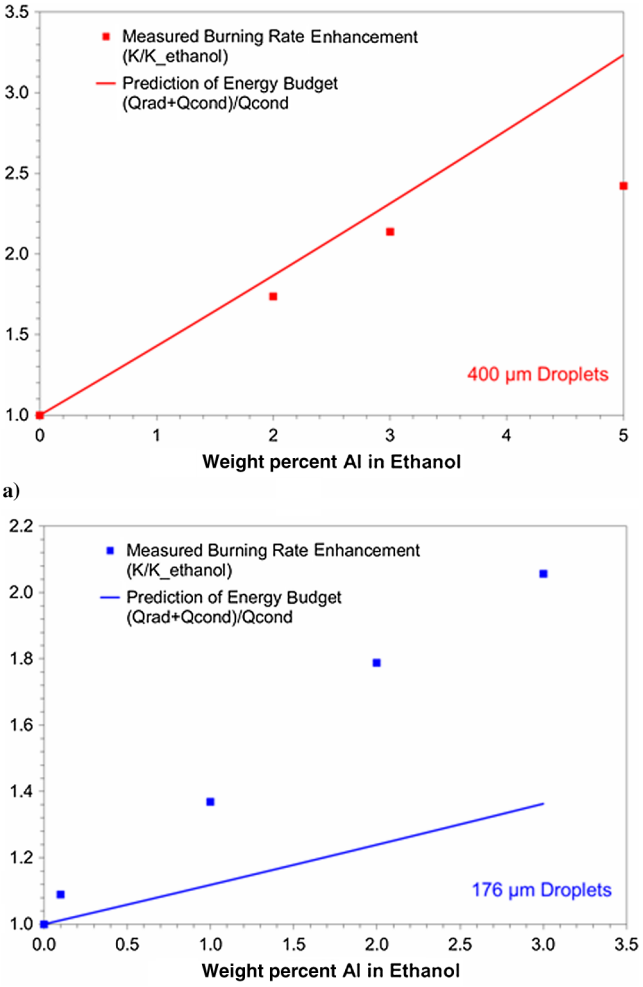

Fig. 10 Ratio $(Q_{\text{rad}} + Q_{\text{cond}})/Q_{\text{cond}}$ in perspective of burning rate enhancement a) 400 μm droplets and b) 176 μm droplets.

the incident radiation. This shows that most of the radiation was absorbed by the Al particles within the nanofluid. The use of the optically thin model can be justified, since the criteria $K_p L \ll 1$ (K_p-absorption coefficient, L distance from the flame to droplet surface) satisfies for our droplet combustion [26].

Based on the model, we calculated the conductive and radiative heat transfer entering the droplet from the flame at varying particle concentrations. Figure 10 shows the ratio of the total heat entering the droplet ($Q_{\text{rad}} + Q_{\text{cond}}$) to Q_{cond} as a function of particle concentration for the 400 and 176 μm droplets, respectively. Also plotted is the measured burning rate enhancement (relative to pure ethanol) for both droplet sizes. As the particle concentration increases, the amount of radiation absorbed by the particles suspended in the droplet increases linearly. This additional energy is available for vaporization at the droplet surface, and we can assume that the droplet-burning rate is proportional to the total heat transfer energy from the flame to the droplet. For the 400 μm droplets (Fig 10a), the ratio of ($Q_{\text{rad}} + Q_{\text{cond}}$) to Q_{cond} agrees well with the measured burning rate increase at all particle concentrations, except for the 5 wt % Al addition. This confirms that radiation absorption by the particles is the main reason for the higher droplet-burning rate for these droplets. At a 5% Al addition, the calculated energy ratio is higher than the measured burning rate increase. This is due to the fact that the burning rate enhancement because of particle radiation absorption has been counteracted by the evaporation suppression resulting from particle aggregation that has become serious at relatively higher particle concentrations. For the 176 μm droplets, the calculated energy ratio is lower than the actual burning rate increase

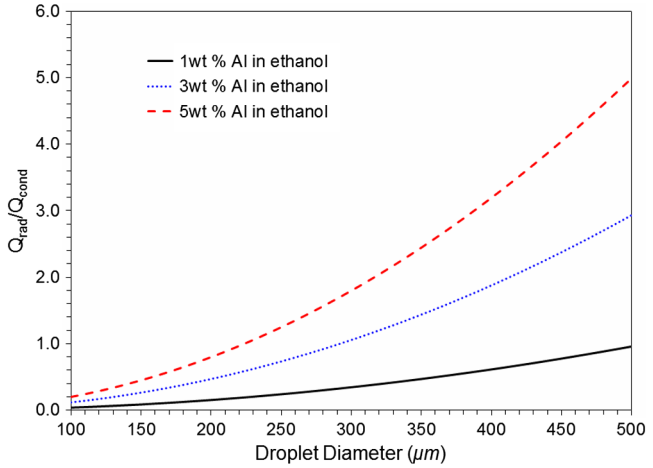

Fig. 11 Variation of the amount of radiation absorbed by the nanofluid droplet as a function of the initial droplet diameter.

at all particle concentrations. This indicates that other mechanisms than radiation absorption of particles also contribute to the droplet-burning rate enhancement.

The results in Fig. 10 show that, for a given particle concentration, the amount of radiation absorbed by the nanoparticles, relative to the heat conduction energy, is a strong function of droplet size. Motivated by this, we plotted the calculated ratio of $Q_{\text{rad}}/Q_{\text{cond}}$ as a function of the initial droplet diameter for various Al concentrations in Fig. 11. The results show that, as the droplet size increases, radiation absorption becomes the dominant source of energy entering into the droplet, hence becoming the main contributor to the enhancement of the burning rate. For smaller droplets, however, it seems that other mechanisms (e.g., surface energy reduction [27–31], enhanced surface area for evaporation due to particle wetting [9–11], and increase in flame temperature [9]) mentioned earlier may be of equal, if not higher, importance than radiation absorption in the enhancement of the burning rate. Nevertheless, the microscale physics at the liquid/gas interface in the presence of nanoparticles needs to be explored further, especially for smaller droplets.

IV. Conclusions

A droplet stream combustion experiment was developed to understand the effect of droplet size on the overall burning behavior of nanofluid fuels (liquid fuels with stable suspensions of energetic nanoparticles), as well as the effect of particle addition on the droplet-burning rate. Ethanol with or without suspension of Al nanoparticles at dilute concentrations (1–5% by weight) were considered. Major conclusions from this work are as follows:

1) Thermophysical properties of the selected nanofluid fuels were measured, including thermal conductivity, viscosity, and surface tension. The results show that a small addition of Al nanoparticles results in a significant increase in the thermal conductivity. The viscosity and surface tension, however, remain nearly unchanged at low concentrations (up to 5 wt%) of Al addition.

2) A macroscopic visualization of the stream flames showed a two-stage burning process: an initial period of pure liquid burning followed by simultaneous burning of both ethanol and Al nanoparticles. A combustion products residue analysis showed that the aggregation intensity increases with increasing particle concentration, but the size of the aggregates remains an order of magnitude smaller than the initial droplet size, indicating that the nanoparticles did not have the chance to form a large aggregate during the droplet-burning process. This allows a more complete combustion of the Al nanoparticles.

3) A small addition of Al nanoparticles can significantly enhance the droplet-burning rate. For example, with a 5 wt% addition of Al nanoparticles in ethanol, the droplet-burning rate increased by 140%. Additionally, a deviation from the classical D^2 law was observed for smaller droplets at relatively higher particle concentrations.

4) A theoretical analysis showed that absorption of radiation energy emitted from the stream flame by the nanoparticles is an important mechanism of energy transfer in nanofluid fuels and cannot be neglected. It is mainly responsible for the burning rate enhancement for large droplets (400 μm). For smaller droplets (176 μm), other mechanisms such as higher flame temperature, enhanced surface area for evaporation due to particle wetting, increased thermal diffusivity of the liquid fuel, and reduction of surface tension and surface energy, all as a result of particle addition, may also contribute to droplet-burning rate enhancement.

Acknowledgments

This work was supported by the National Science Foundation, with Ruey-Hung Chen as the Technical Monitor.

References

[1] Yetter, R. A., Risha, G. A., and Son, S. F., "Metal Particle Combustion and Nanotechnology," *Proceedings of the Combustion Institute*, Vol. 32, No. 2, 2009, pp. 1819–1838. doi:10.1016/j.proci.2008.08.013

[2] Dreizin, E. L., "Metal-Based Reactive Nanomaterials," *Progress in Energy and Combustion Science*, Vol. 35, No. 2, 2009, pp. 141–167. doi:10.1016/j.pecs.2008.09.001

[3] Van Devener, B., Perez, J. P. L., Jankovich, J., and Anderson, S. L., "Oxide-Free, Catalyst-Coated, Fuel-Soluble, Air-Stable Boron Nanopowder as Combined Combustion Catalyst and High Energy Density Fuel," *Energy and Fuels*, Vol. 23, No. 12, 2009, pp. 6111–6120. doi:10.1021/ef900765h

[4] Van Devener, B., and Anderson, S. L., "Breakdown and Combustion of JP-10 Fuel Catalyzed by Nanoparticulate CeO_2 and Fe_2O_3," *Energy and Fuels*, Vol. 20, No. 5, 2006, pp. 1886–1894. doi:10.1021/ef060064g

[5] Tyagi, H., Phelan, P. E., Prasher, R., Peck, R., Lee, T., Pacheco, J. R., and Arentzen, P., "Increased Hot-Plate Ignition Probability for Nanoparticle-Laden Diesel Fuel," *Nano Letters*, Vol. 8, No. 5, 2008, pp. 1410–1416. doi:10.1021/nl080277d

[6] Beloni, E., Hoffmann, V. K., and Dreizin, E. L., "Combustion of Decane-Based Slurries with Metallic Fuel Additives," *Journal of Propulsion and Power*, Vol. 24, No. 6, 2008, pp. 1403–1411. doi:10.2514/1.28042

[7] Allen, C., Mittal, G., Sung, C. J., Toulson, E., and Lee, T., "An Aerosol Rapid Compression Machine for Studying Energetic-Nanoparticle-Enhanced Combustion of Liquid Fuels," *Proceedings of the Combustion Institute*, Vol. 33, No. 2, 2011, pp. 3367–3374. doi:10.1016/j.proci.2010.06.007

[8] Rotavera, B., Kumar, A., Seal, S., and Petersen, E. L., "Effect of Ceria Nanoparticles on Soot Inception and Growth in Toluene-Oxygen-Argon Mixtures," *Proceedings of the Combustion Institute*, Vol. 32, No. 1, 2009, pp. 811–819. doi:10.1016/j.proci.2008.07.024

[9] Sabourin, J. L., Yetter, R. A., Asay, B. W., Lloyd, J. M., Sanders, V. E., Risha, G. A., and Son, S. F., "Effect of Nano-Aluminum and Fumed Silica Particles on Deflagration and Detonation of Nitromethane," *Propellants, Explosives, Pyrotechnics*, Vol. 34, No. 5, 2009, pp. 385–393. doi:10.1002/prep.v34:5

[10] Sabourin, J. L., Yetter, R. A., and Parimi, V. S., "Exploring the Effects of Nanostructured Particles on Liquid Nitromethane Combustion," *Journal of Propulsion and Power*, Vol. 26, No. 5, 2010, pp. 1006–1015. doi:10.2514/1.48579

[11] McCown, K. W., III, and Petersen, E. L., "Effects of Nano-Scale Additives on the Linear Burning Rate of Nitromethane," *Combustion and Flame*, Vol. 161, No. 7, 2014, pp. 1935–1943. doi:10.1016/j.combustflame.2013.12.019

[12] Gan, Y. A., Lim, Y. S., and Qiao, L., "Combustion of Nanofluid Fuels with the Addition of Boron and Iron Particles at Dilute and Dense Concentrations," *Combustion and Flame*, Vol. 159, No. 4, 2012, pp. 1732–1740. doi:10.1016/j.combustflame.2011.12.008

[13] Gan, Y. A., and Qiao, L., "Combustion Characteristics of Fuel Droplets with Addition of Nano and Micron-Sized Aluminum Particles," *Combustion and Flame*, Vol. 158, No. 2, 2011, pp. 354–368. doi:10.1016/j.combustflame.2010.09.005

[14] Gan, Y. A., and Qiao, L., "Evaporation Characteristics of Fuel Droplets with the Addition of Nanoparticles Under Natural and Forced Convections," *International Journal of Heat and Mass Transfer*, Vol. 54, Nos. 23–24, 2011, pp. 4913–4922. doi:10.1016/j.ijheatmasstransfer.2011.07.003

[15] Gan, Y. A., and Qiao, L., "Optical Properties and Radiation-Enhanced Evaporation of Nanofluid Fuels Containing Carbon-Based Nanostructures," *Energy and Fuels*, Vol. 26, No. 7, 2012, pp. 4224–4230. doi:10.1021/ef300493m

[16] Ghadimi, A., Saidur, R., and Metselaar, H. S. C., "A Review of Nanofluid Stability Properties and Characterization in Stationary Conditions," *International Journal of Heat and Mass Transfer*, Vol. 54, Nos. 17–18, 2011, pp. 4051–4068. doi:10.1016/j.ijheatmasstransfer.2011.04.014

[17] Tanvir, S., and Qiao, L., "Surface Tension of Nanofluid-Type Fuels Containing Suspended Nanomaterials," *Nanoscale Research Letters*, Vol. 7, No. 1, 2012, pp. 226–235. doi:10.1186/1556-276X-7-226

[18] Botero, M. L., Huang, Y., Zhu, D. L., Molina, A., and Law, C. K., "Droplet Combustion of Ethanol, Diesel, Castor Oil Biodiesel, and Their Mixtures," *7th U.S. National Combustion Meeting of the Combustion Institute*, Georgia Inst. of Technology, Atlanta, 2011, Paper 1D07.

[19] Botero, M. L., Huang, Y., Zhu, D. L., Molina, A., and Law, C. K., "Synergistic Combustion of Droplets of Ethanol, Diesel and Biodiesel Mixtures," *Fuel*, Vol. 94, No. 1, 2012, pp. 342–347. doi:10.1016/j.fuel.2011.10.049

[20] Takahashi, F., Dryer, F. L., and Williams, F. A., "Combustion Behavior of Free Boron Slurry Droplets," *Proceedings of the Combustion Institute*, Vol. 21, No. 1, 1986, pp. 1983–1991. doi:10.1016/S0082-0784(88)80435-1

[21] Virepinte, J. F., Biscos, Y., Lavergne, G., Magre, P., and Collin, G., "A Rectilinear Droplet Stream in Combustion: Droplet and Gas Phase Properties," *Combustion Science and Technology*, Vol. 150, Nos. 1–6, 2000, pp. 143–159. doi:10.1080/00102200008952121

[22] Okajima, S., and Kumagai, S., "Further Investigations of Combustion of Free Droplets in a Freely Falling Chamber Including Moving Droplets," *Proceedings of the Combustion Institute*, Vol. 15, No. 1, 1975, pp. 401–407. doi:10.1016/S0082-0784(75)80314-6

[23] Law, C. K., "Recent Advances in Droplet Vaporization and Combustion," *Progress in Energy and Combustion Science*, Vol. 8, No. 3, 1982, pp. 171–201. doi:10.1016/0360-1285(82)90011-9

[24] Chen, Z., and Ju, Y., "Theoretical Analysis of the Evolution from Ignition Kernel to Flame Ball and Planar Flame," *Combustion Theory and Modeling*, Vol. 11, No. 3, 2007, pp. 427–453. doi:10.1080/13647830600999850

[25] Tien, C. L., "Thermal Radiation Properties of Gases," *Advances in Heat Transfer*, Vol. 5, No. 3, 1969, pp. 253–324. doi:10.1016/S0065-2717(08)70131-X

[26] Liu, Y., and Rogg, B., "Prediction of Radiative Heat Transfer in Laminar Flames," *Combustion Science and Technology*, Vol. 118, Nos. 1–3, 1996, pp. 127–145. doi:10.1080/00102209608951975

[27] Freire, M. G., Carvalho, P. J., Fernandes, A. M., Marrucho, I. M., Queimada, A. J., and Coutinho, J. A. P., "Surface Tensions of Imidazolium Based Ionic Liquids: Anion, Cation, Temperature and Water Effect," *Journal of Colloid and Interface Science*, Vol. 314, No. 2, 2007, pp. 621–630. doi:10.1016/j.jcis.2007.06.003

[28] Vargaftik, N. B., Volkov, B. N., and Voljak, L. D., "International Tables of the Surface-Tension of Water," *Journal of Physical and Chemical Reference Data*, Vol. 12, No. 3, 1983, pp. 817–820. doi:10.1063/1.555688

[29] Vazquez, G., Alvarez, E., and Navaza, J. M., "Surface-Tension of Alcohol Plus Water from 20 to 50°C," *Journal of Chemical and Engineering Data*, Vol. 40, No. 3, 1995, pp. 611–614. doi:10.1021/je00019a016

[30] Chen, R. H., Phuoc, T. X., and Martello, D., "Surface Tension of Evaporating Nanofluid Droplets," *International Journal of Heat and Mass Transfer*, Vol. 54, Nos. 11–12, 2011, pp. 2459–2466. doi:10.1016/j.ijheatmasstransfer.2011.02.016

[31] Chen, R., Phuoc, T. X., and Martello, D., "Effects of Nanoparticles on Nanofluid Droplet Evaporation," *International Journal of Heat and Mass Transfer*, Vol. 53, Nos. 19–20, 2010, pp. 3677–3682. doi:10.1016/j.ijheatmasstransfer.2010.04.006

J. Oefelein
Associate Editor